NTNU
Kunnskap for en bedre verden

Department of Geoscience and Petroleum

TPG 4560 - Petroleum Engineering, Specialization Project

Exploring the Impact of Thermal Considerations on CO2 Plume Shape and Sensitivity Studies

Author:
Alireza Mohsenifesegandis

Autumn 2023

Table of Contents

List of Figures

List of Tables

1 Introduction

1.1 Global Warming

One of the most important environmental issues of the modern man is the global warming. Global warming has undeniable effects on the human life, natural ecosystem, and climate. Climate changes like frequent heat waves, higher precipitation, and more frequent and intense climate events are in this category [8]. The Earth Atmosphere consists of different gases, some of these gases like, Carbon dioxide, Methane, and Nitrous oxide trap heat in the atmosphere, and lead to higher surface temperature. Since the industrial revolution, the amount green house gases emitted to the atmosphere has increased significantly due to burning fossil fuels, and less carbon dioxide is absorbed by the forests because of deforestation in large scales. This has ended up in the higher temperature on the planet surface. Figure 1 shows the global land and ocean September temperature anomalies from 1850 till 2023.(data from national centers for environmental information)

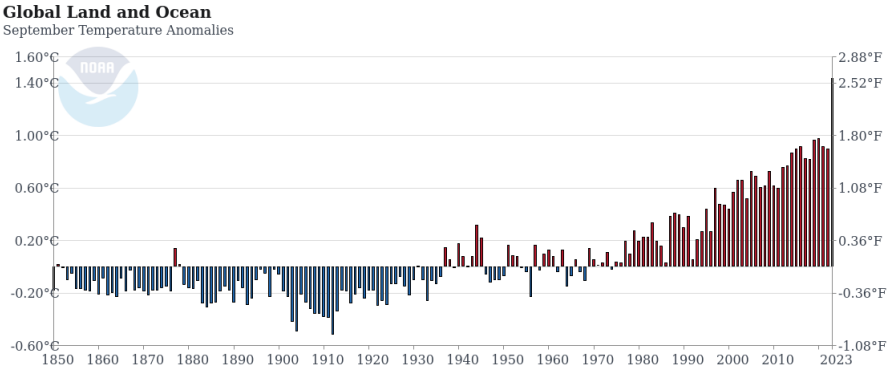

Figure 1: Global land and ocean temperature since 1850

This challenge can be solved by storing CO_2 under the surface in the deep geological formations, using renewable energy sources instead of fossil fuels, and more efficient energy consumption by human beings.

1.2 CO_2 Sequestration

Fossil fuels are at least producing the world's 80% energy [15]. Moving from fossil fuels to renewable energies cannot happen immediately. Industries, transportation, and agriculture are highly dependent on fossil fuels. Moreover, renewable energy sources, like wind, solar, and biofuels are intermittent, so they need to be stored, which is a challenge. [18] Global emission reduction can not be reached by only using renewable energy resources instead of fossil fuels, or storing CO_2 underground. As first proposed by Pacala and Socolow), the wedge model approach could be a solution.[16] In this approach, numerous activities work together to make a significant effect. There are several versions of wedge models with different proposed activities. Some of the activities which are in most of the models are, increased energy efficiency, new renewable energy sources, moving from coal to gas, carbon capture and storage, and nuclear energy. CO_2 sequestration is defined as injecting Carbon dioxide into the geological rock formations, which could be either layers bearing hydrocarbon or saline aquifers for long periods. There are numerous successful CO_2 sequestration projects around the world. The first commercial CCS project, Sleipner started in 1996 in the North Sea, Norway, and injected one million tons of carbon dioxide underground.[19] With more than 25 years of injection can ensure that this approach combined with other approaches can be one of the solutions to overcome global warming.

1.3 Research Objectives

As explained in the first part of the introduction, CO_2 sequestration is one of the several solutions, that can help the world overcome the global warming problem alongside the other solutions. CO_2 properties like its density and viscosity which play an important role in the plume movement, are highly dependent on the pressure and temperature. In most of the previous studies, thermal effects are neglected. In this study using the reservoir simulator, pflotran-OGS, thermal effects will be studied. Different cases, which have variations in the injection temperature, injection pattern, injection well placement, presence of impermeable horizontal layers, and injection rate will be studied in both thermal and isothermal modes. The effect of these factors on plume shape after different times, the amount of CO_2 in different phases, and the time in which the plume reaches the license boundary should be studied.

Real-world cases have so many uncertainties, and heterogeneity. These factors have great influences on the results and make the result processing and understanding of the different effects hard. To better understand, and easier interpretation, a simple case will be used as the target formation.

2 Theory

2.1 Trapping Mechanisms

Carbon dioxide is injected in supercritical form, and stored in the interconnected pore system. After injection, Carbon dioxide starts moving in the system due to pressure difference, or gravitational forces. The injected CO_2 will be trapped due to different mechanisms, which could be physical or chemical, which controls the CO_2 leakage, too. Physical and chemical trapping mechanisms occur simultaneously but in different time scales. Table 1 summarizes these mechanisms. In this section, these mechanisms are briefly explained.

Physical	Chemical
Stratigraphic and Structural	Dissolution
Hydrodynamic	Mineralization
Residual	

Table 1: Trapping Mechanisms

2.1.1 Stratigraphic and Structural

This mechanism works exactly the same as the trapping mechanism for hydrocarbon reservoirs. An impermeable layer which could be a shale layer or a salt bed overlying a permeable zone. CO_2 is injected in a supercritical state, and its density is between 450 to 900 kg/m3 [6], which is by the way highly dependent on the pressure and temperature. Fluid with the lower density, which is CO_2 in this case, moves upwards. Due to the very low permeability of the overlying layer or very high entry pressure, which is due to very small pore size, fluid is stopped and trapped. This mechanism plays an important role in the early stages of the injection.[18]

2.1.2 Hydrodynamic

Hydrodynamic trapping occurs in saline formations lacking a closed trap, where fluids migrate at a gradual pace across extensive distances. When CO_2 is introduced into a reservoir, it tends to displace saline water primarily at the formation's top due to gravitational forces arising from the density disparity between CO_2 and brine. CO_2 persists in migration as a distinct phase atop the formation until it becomes entrapped within local stratigraphical or structural traps within the sealing formation or attains residual CO_2 saturation in areas where brine displaces the injected CO_2 during the imbibition process. A substantial quantity of CO_2 undergoes dissolution in the formation water (brine) phase over an extended temporal scale. If the distance from the injection point to the termination of the impermeable formation overhead spans hundreds of kilometers, millions of years are requisite for the fluid to ascend from the deep basin to the surface.[10]

2.1.3 Residual

One well-known phenomenon in the oil and gas industry, which has considerable influence on the recoverable amount of hydrocarbon in oil and gas-bearing formations is residual trapping. As the non-wetting phase moves in the rock which was initially filled with the wetting phase, the plume of the secondary fluid doesn't move as a whole. Due to residual trapping, a specific amount of fluid will be trapped in the pores. The magnitude of residual trapping is a function of the pore throat size, the interfacial tension, and the wettability. In CO_2 sequestration in sandstone reservoirs, CO_2 is the non-wetting phase, and the brine is the wetting. [9][17].

2.1.4 Dissolution

Carbon dioxide naturally exists in the subsurface, which could be in the form of dissolved CO_2 in water, or as free gas which can move in the pore system. CO_2 in the subsurface could come from different sources, like volcanic systems, and organic sources. The organic matter being decomposed, microbes producing CO_2 as a byproduct, degradation in hydrocarbon fields, oxidation of oil and gas, and decabonation of marine carbonates could be the sources of the carbon dioxide in the subsurface. [2]

Injected CO_2 moves to the top of the permeable layer, and will be stored there. The CO_2 plume will be in contact with the brine and will start dissolving in the aqueous phase. Dissolution of CO_2 in the brine is due to diffusion and convection, and convection determines the rate of the process. This process is slower in comparison to physical storage mechanisms, but more important and ensuring in the long term.

2.1.5 Mineralization

Dissolved CO_2 in the brine makes the environment acidic. While the acidic phase is in contact with the grains and the elements present in the rock, they react and start to deposit. This mechanism is dominant in the late-time storage phases, even after dissolution.

2.2 CO2 Properties

With a density of 1.87 kg/m^3 at atmospheric conditions, CO2 is a thermodynamically stable gas that is heavier than air and compressible. CO_2 properties are functions of pressure and temperature. In deep saline aquifers, due to overburden pressure, and thermal gradient, both the pressure and temperature are high. In this circumstance, CO_2 will be in a liquid phase. After the critical point, CO_2 will move to a supercritical state, which can have a density variation between 150 to around 800 Kg/m^3. The critical point for CO_2 is at T = 30.98 $^\circ C$, P = 73.8 bar. CO_2 viscosity also changes significantly with pressure and temperature. In the liquid phase, it can have a viscosity of 0.18 cP, and in the gas phase, it could be as low as 0.02 cP. [21]

2.3 Thermal Effects

As mentioned in the previous part, CO_2 properties changes dramatically with pressure and temperature. In CO_2 sequestration projects, injection temperature can vary depending on different factors like the ambient temperature, and the transportation system, in pipeline transportation the temperature could be very low. There are three moving fronts, pressure front, free gas front, and temperature. Rocks have a big surface-to-volume ratio, so the injected CO_2 will quickly reach a thermal equilibrium with the surrounding rock. This temperature change has a great effect on the gas properties, and this difference can influence the viscous movement and the buoyancy effects. [11]

2.4 Plume Shape

Understanding the plume shape and how the free gas propagates in the sedimentary basins is crucial. Injected CO_2 will be lighter than the initial fluid, which could be brine in saline aquifers, or oil if the target formation is a depleted reservoir. CO_2 with lower density will reside in the shallowest part of the formation below the impermeable layer. So the potential for upward leakage will be enhanced and it should be addressed. On the other hand, CO_2 can leak from the existing infrastructure, like abandoned wells. Every well that the free gas reaches is a high-risk conduit that can let the CO_2 come back to the surface, which is against the regulatory rules.

There are several analytical and semi-analytical solutions to find the plume shape and its extent in the formation. Real-life cases have a high range of uncertainty and heterogeneity. These solutions can approximate the plume shape while excluding many factors, and with the help of simplifications. The other solution to this question is the numerical solution, which could be more realistic in real-life cases, and include most of the reservoir and fluid characteristics, and fewer simplifications.

2.4.1 Analytical and Semi-analytical Solutions

Under reasonably moderate assumptions concerning fluid characteristics and the displacement process, Nordbotten et al. developed an analytical solution to depict the temporal and spatial progression of the CO_2 plume. This solution is based on energy minimization principles and simplifies into a straightforward radial expression reminiscent of the Buckley–Leverett solution under circumstances characterized by viscous dominance.[14]

In 2006, Nordbotten and Celia took advantage of similarity solutions and included slight miscibility between the two fluids, CO_2 and brine, and compressibility in both of the fluid phases. Moreover, the solution offers information about where the interface lies between the two fluids, along with the formation of drying fronts within the injected fluid.[13]

In 2009, Dentz and Tartakovsky based on the Dupuit approximation and explicitly incorporated buoyancy effects, formulated an approximate analytical solution that characterizes the dynamics of the interface when injecting supercritical carbon dioxide into homogeneous geological formations. Their solution was not limited to saline aquifers and applied to reservoirs with a lighter host fluid, like methane.[3]

Influences of fine-scale capillary forces in the integrated equations were added in 2011 by Nordbotten and Dahle. [12]

Including the CO_2 compressibility and buoyancy effects in the injection well Vilarrasa et al. developed a semi-analytical solution for the CO2 plume geometry and fluid pressure evolution. Using this solution the assumption of uniformly injected CO_2 along the aquifer thickness is removed. [22]

Wu et al. derived a novel equation for complex fluid movement in the porous media, rooted in the equation of continuity and the generalized Darcy's law. [7]

2.4.2 Numerical Solutions

Numerical methods play a critical role in calculating the CO_2 plume shape within sedimentary basins. These approaches involve the use of computational models to simulate fluid dynamics, transport phenomena, and geologic characteristics. Employing iterative algorithms and discretizing the governing equations, numerical simulations can provide beneficial information into the evolution of the CO_2 plume over space and time. These methods take into account various factors, including fluid properties, rock permeability, rock compressibility, capillary pressures, and the injection process. Numerical methods can solve the equations using finite difference, finite element, or other numerical techniques. Research on numerical approaches remains at the forefront as computer capabilities grow. There are numerous reservoir simulators, and most of these simulators are initially developed for oil and gas reservoir goals, but with some customization, they can be used for CO_2 and brine cases.

3 Methods

In this section, the reservoir simulator which will be used, and the simple reservoir model that is the target formation will be discussed. Among different reservoir simulators, which are almost using the same set of equations, pflotran-OGS is chosen to be used in this study.

3.1 Pflotran-OGS

US labs started the Pflotran Parallel Flow Transport Simulator is an Open Source project, with a background in environmental science and groundwater flow. OpenGoSim has developed a reservoir simulator capability that is optimized for Carbon Capture and Storage(CCS), called pflotran-OGS. Pflotran-OGS is mainly modern Fortran, Petsc and Hypre are largely C, some C++, and Python. Pflotran-OGS solves the flow equations fully implicit and uses the two-point flux approximation. This simulator has different modes that can be used based on the case that is being studied. [1]

- Gas-Water Mode
- Compositional Modes
    1. COMP3
    2. COMP4
    3. Full compositional

For CO_2 injection in the saline aquifers, Gas-water Mode is the best fit, and describes a two-phase flow model. Compositional Modes can handle more than two phases in the reservoir. COMP3 is used for CO_2, reservoir gas, and water. For cases with both reservoir oil and gas, COMP4 solution mode must be used. Gas-Water solution mode will be used in this study.

3.1.1 Gas-Water Mode

As mentioned previously, in the Gas-Water Mode describes a two-phase flow model. In this module, each of the components could be in both phases, so CO_2 can be dissolved in the aqueous phases, and water can be evaporated in the gas phase. The molar balance equation is solved for each component, and for the thermal effects, the energy equation is used. Equation 1 describes the molar balance for each phase. In which, α is the phase, gas, or water, and β is the component, aqueous or vapor.

$$\frac{\partial}{\partial t}\phi \sum_{\beta}(x_{\beta}^{\alpha} S_{\beta}\eta_{\beta}) + \nabla \cdot \sum_{\beta}(x_{\beta}^{\alpha} q_{\beta}\eta_{\beta} + \phi S_{\beta} D_{\beta}\eta_{\alpha}\nabla x_{\beta}^{\alpha}) = Q_i \tag{1}$$

Where:

- ϕ is porosity;
- x_{β}^{α} is mole fraction of α in the phase β;
- S_{β} represents the saturation of phase β;
- η_{β} is molar density of phase β;
- q_{β} is the Darcy velocity of the phase β;
- D_{β} is the diffusion coefficient of phase β;
- Q_i is a source term.

```
import sys
stdoutOrigin=sys.stdout
sys.stdout = open("COORDF.txt", "w")
print('COORD')
NJ= 20   #number of cells in J direction
NI= 20   #number of cells in I direction
X= 200   #Cell size in X direction
Y= 200   #Cell size in Y direction
Zmin= 0 #minimum depth
Zmax=  10000 #maximum depth
for j in range(NJ+1):

    for i in range(NI+1):



        print(str(i*X) + ' ' + str(j*Y)+ ' '+ str(Zmin)+' ' + str(i*X) + ' ' + str(j*Y)+ ' '+str(Zmax))


print('/')

sys.stdout.close()
sys.stdout=stdoutOrigin

```

Figure 2: Codes for generating COORD

For phase β, the Darcy velocity is calculated as below:

$$q_\beta = \frac{K k_\beta}{\mu_\beta} \nabla (P_\beta - \rho_\beta g z) \tag{2}$$

In equation 2, K is rock permeability, k_β, μ_β, P_β, ρ_β are the relative permeability, viscosity, pressure and density of the phase β respectively, g is gravitational constant, and z is height. In pflotran-OGS, the default mode is non-isothermal, and equation 3 shows the energy balance, in which the internal energy of each phase, density, heat capacity, and thermal conductivity of the formation is used.

$$\frac{\partial}{\partial t}[\phi \sum_\beta S_\beta \eta_\beta U_\beta + (1-\phi)\rho_r c_r T] + \nabla \cdot \sum_\beta [q_\beta \eta_\beta H_\beta + \kappa \nabla T] = Q_e \tag{3}$$

For CO_2 properties the Span and Wagner[20] correlation is used in Pflotran-OGS, and the simulator uses he Duan, Sun and the Sun, Duan, Hu, Li, Mao correlations for the properties of the CO2-H2O and CO2-H2O-NaCl systems. [4] [5]

3.2 Reservoir Model

As mentioned in the Introduction section, a simple reservoir model will be used in this study. The target reservoir in this study is similar to the model in the pflotran-OGS tutorial with some changes. The model area is 4000 meters in 4000 meters and has a thickness of 160 meters. In X and Y directions, grid cells are all equal in size, consisting of 400 cells in each layer, with a size of 200 in 200 meters. In the Z-direction, there are 160 cells with a constant thickness of 1 meter. The original model in the tutorial is horizontal, using the codes in figures 2 and 3 the model became shallower in the Northern part and deeper in the Southern part. The shallowest part of the reservoir is at a depth of 1150 meters, and the deepest part lies at 1368 meters.

A porosity value of 0.3 is set for all of the 64000 cells. In the case of permeability, total permeability in the X and Y directions is equal. Horizontal permeability is 300 millidarcy, but using the keyword DPCF, a heterogeneous permeability distribution is generated using the Dystra-Parsons standard distributionadd reference here. The given value for DPCF in this study is 0.2, which corresponds to a slightly heterogeneous reservoir. Layers 1 and 16 in the Z-direction have zero permeability in all directions. The ratio of vertical to horizontal permeability is set to 0.1. Figure 4 shows the permeability distribution in the reservoir. Material and fluid properties used in this model are listed in the table 2 and 3 respectively.

A vertical well is used for CO_2 injection. The average field pressure before injection starts is 120 Bar and the Bottom-hole pressure limit is set to 1000 Bar. The injection is at the temperature of $15^{\circ}C$, and the injection target is set to 0.25 Million tons per year. The injection location is at cell [11,11] and the well is perforated between layers 90 and 130 in vertical direction.

```python
import sys
stdoutOrigin=sys.stdout
sys.stdout = open("ZCORNF.grdecl", "w")
print('ZCORN')
Dshallow = 1150 # shallowest point
dz=1
dzdy=3
NJ= 20   #number of cells in J direction
NI= 20   #number of cells in I direction
NK=160   #number of cells in K direction
corI=2*NI
corII=4*NI

D=Dshallow
print(str(corI)+'*' + str(D))
D=D+dzdy
for i in range(NJ-1):
    print(str(corII)+'*' + str(D))
    D=D+dzdy
print(str(corI)+'*' + str(D))

D=Dshallow+dz
for i in range(NK-1):

    for k in range(2):
        ND=D
        print(str(corI)+'*' + str(ND))
        ND=ND+dzdy
        for K in range(19):
            print(str(corII)+'*' + str(ND))
            ND=ND+dzdy
        print(str(corI)+'*' + str(ND))
    D+=dz
print(str(corI)+'*' + str(D))
D=D+dzdy
for i in range(NJ-1):
    print(str(corII)+'*' + str(D))
    D=D+dzdy
print(str(corI)+'*' + str(D))
print('/')

sys.stdout.close()
sys.stdout=stdoutOrigin
```

Figure 3: Codes for generating ZCORN

Property	Value	Unit
Rock Density	2350	kg/m^3
Specific heat	1000	J/kg.C
Thermal conductivity dry	1.6	W/m.C
Thermal conductivity wet	4.3	W/m.C
Rock Compressibility	4.35×10^{-5}	1/Bar

Table 2: Material Properties

Property	Value	Unit
Liquid diffusion coefficient	2.0×10^{-9}	m^2/s
Gas diffusion coefficient	2.0×10^{-5}	m^2/s
Brine Salinity	1.0	Molal
Water surface density	1000	kg/m^3
Gas Surface density	1.8	kg/m^3

Table 3: Fluid Properties

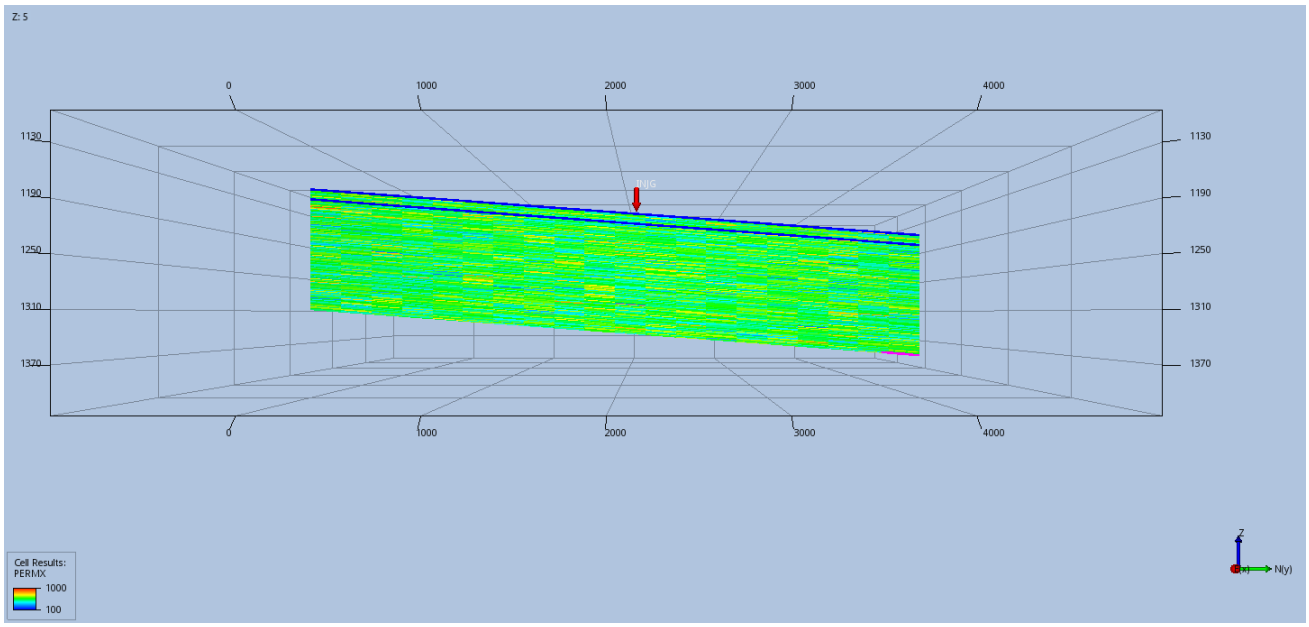

Figure 4: Permeability distribution

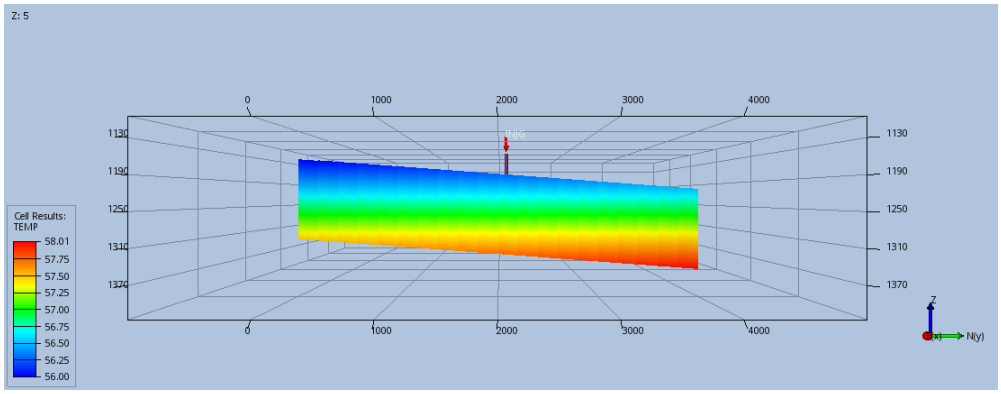

Figure 5: Initial temperature distribution in the reservoir

3.3 Sensitivity Analysis

In the Reservoir Model section, the base case was explained. In this section, different scenarios will be illustrated, to see their effect on different parameters, like plume shape, time to reach the license boundary, etc.

3.3.1 Injection temperature

As mentioned in the previous sections, CO_2 properties, density, and viscosity are functions of pressure and temperature, and variations in these parameters can change the plume propagation in both horizontal and vertical directions. Moreover, when injected CO_2 is colder than the brine in the aquifer, the temperature front moves away from the injection point with time, and the brine around the well becomes colder. Gas solubility in brine is also a function of temperature. Consequently, the amount of free CO_2 in the reservoir might vary with the changes in injection temperature. In this study, injection temperatures of 15, 30, 40, and 50 °C are studied. The ambient reservoir temperature varies between 56 and 58 degrees Centigrade. Figure 5 shows the temperature variation in the reservoir.

```
import sys

stdoutOrigin=sys.stdout
sys.stdout = open("log.inc", "w")
for i in range(511):

        print('  TIME '+ str(i*5*2-5) + ' d\n' +'  OPEN\n'+'  TIME '+ str(i*5*2) + ' d\n' +'  SHUT')

sys.stdout.close()
sys.stdout=stdoutOrigin


```

Figure 6: Codes for opening and shutting well

3.3.2 Injection Pattern

CO_2 is captured in different sites, pressurized, and sent to the injection point. Captured CO_2 could be sent to injection wells via pipelines, or ships might be used for this purpose. In the case of using a ship, the injection might not be consistent, meaning that, the ship might be at the injection point for a couple of days, and away for some other days, this case is called periodic injection, in this study. To simulate this case, the injection well will be open for 5 days and shut for 5 days. This pattern will continue for 14 years. Figure 6 shows the used codes for this purpose.

3.3.3 Brine Salinity

Brine salinity has effects both on the brine properties, viscosity, and density, and also affects the amount of dissolved CO_2 in the brine. Higher salinity increases the brine density and viscosity, and higher brine density changes the buoyancy effects and alters the free CO_2 ascending. Higher viscosity influences the capillary movement of the brine which changes the plume shape. In this study, three different values for brine salinity are studied, 1.0, 1.2, and 1.4 Molal.

3.3.4 Permeability Anisotropy

In most of cases, due to the overburden pressure, permeability in the Z-direction is less than the horizontal permeability. The higher the vertical permeability, the easier the free gas moves upwards. Even in most realistic cases, the value for the vertical permeability is missing, and a ratio is used to convert the horizontal permeability to vertical permeability. In this study, four values for Kv/Kh are studied. As mentioned previously in this section, for the base case, the value of Kv/Kh is set to 0.1. The other three values are 0.3, 0.5, and 0,7.

3.3.5 Impermeable layers

Presence of thin impermeable layers, like calcite layers or shales within the sedimentary basin is common, which can have great effects on the plume shape, and how the CO_2 ascends. These layers could be fully or partially impermeable. Moreover, they could be present everywhere, or just in some places. To study the effect of impermeable layers, two different scenarios were made, in the first case, there are two fully impermeable layers, in the depth equivalent to layers 100 and 105. The zone between these two layers has a higher permeability in comparison to the rest of the reservoir. That is the reason that these layers are named thief zones. The second case is similar to the first case, but the upper impermeable layer has a small opening at the shallowest part. This opening, or chimney, has several effects. The first is the pressure communication between the thief zone and the shallower part of the injection zone, And the second possible effect is that after the injected CO_2 reaches the chimney, it can move upwards to the shallower part, which increases the amount of CO_2 that could be injected in that layer. The third which can be more important than others is the reaching time to the boundary. Moreover, in thermal runs, if this chimney is close to the injection point, CO_2 can find a way to shallower parts, and due to the higher $CO_2 - brine$ density

difference, free gas can move to the reservoir top even faster. Figure 7 shows the transmissibility in the Z-direction for the whole system and the upper impermeable layer.

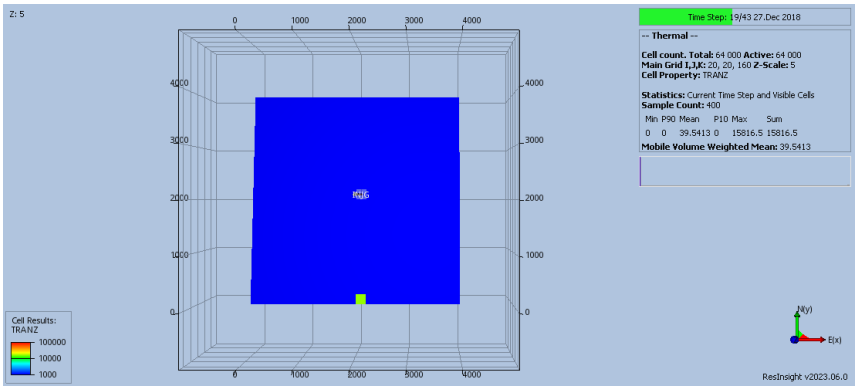

Top View

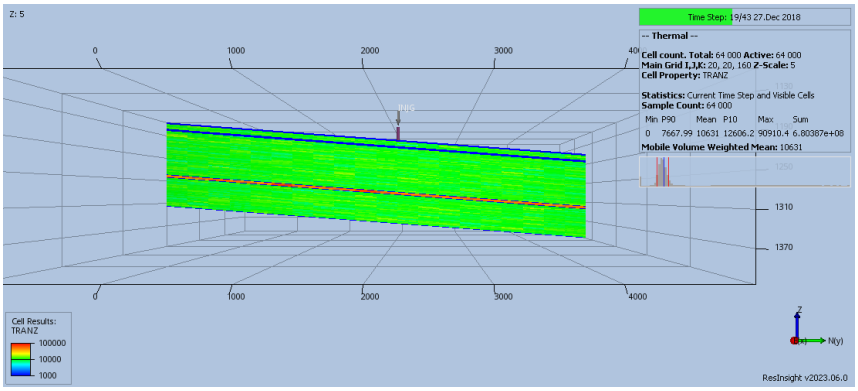

Side View

Figure 7: Transmissibility in the Z-direction

3.4 Reach Time

One of the important aspects of the CO_2 sequestration projects is the storage capacity, which should be calculated before the project. Storage capacity is a function of different properties like porosity, irreducible water saturation, reservoir area, and thickness. One more thing that should be taken into account, is the time by which the free gas reaches the reservoir boundaries. This could be affected by thief zones, faults, etc. To calculate this time a Python code was developed that calculates the amount of free gas in each cell, and sums up the values for the cells which are in the reservoir boundary. Time step in which this sum is bigger than a cut-off value will be announced as reach time. The code is in the figure 9.

3.5 Plume Profile

To study the plume shape and profile in each time step, software can be used. To have a very quick understanding of the plume profile, which is not as comprehensive as software, and does not include all the details, a Python code is generated. This code makes cross-sections in one direction and calculates the amount of free gas in that cross-section. This code can be used to compare two plume shapes in different time steps. The code is shown in the figure 16.

```python
from ecl2df import grid, EclFiles,summary
import matplotlib.pyplot as plt
import numpy as np
import os
def reachtime(address, filename):

    os.chdir(str(address))
    eclfiles = EclFiles(str(filename))
    df = grid.df(eclfiles, rstdates='all')
    times=['2000-01-01','2000-12-31','2001-12-31','2002-12-31','2003-12-31',
        '2004-12-30','2005-12-30','2006-12-30','2007-12-30','2008-12-29',
        '2009-12-29','2010-12-29','2011-12-29','2012-12-28','2013-12-28',
        '2014-12-28','2015-12-28','2016-12-27','2017-12-27','2018-12-27',
        '2019-12-27','2020-12-26','2021-12-26','2022-12-26','2023-12-26',
        '2024-12-25','2025-12-25','2026-12-25','2027-12-25','2028-12-24',
        '2029-12-24','2039-12-22','2049-12-19','2059-12-17','2069-12-14',
        '2079-12-12','2089-12-09','2099-12-07']


    for t in times:
        mat=df[['I', 'J', 'K', 'SGAS@'+t,'PORV']].to_numpy()
        temp= mat[mat[:, 1] == 1]
        temp=np.c_[ temp, np.zeros(np.shape(temp)[0]) ]
        temp[:,5]=temp[:,3]*temp[:,4]
        SUM=np.sum(temp,axis=0)

        if (SUM[5]>0.01):
            TIME=t
            print(TIME)
            break


```

Figure 8: reach time code

```python
def profiletwo(address,folder1,folder2, filename):
    os.chdir(str(address)+str(folder1))
    eclfiles = EclFiles(str(filename))
    df1 = grid.df(eclfiles, rstdates='all')

    os.chdir(str(address)+str(folder2))
    eclfiles = EclFiles(str(filename))
    df2 = grid.df(eclfiles, rstdates='all')

    times=['2000-01-01','2000-12-31','2001-12-31','2002-12-31','2003-12-31','2004-12-30','2005-12-30','2006-12-30','2007-12-30','2008-12-29','2009-12-29',
        '2010-12-29','2011-12-29','2012-12-28','2013-12-28','2014-12-28','2015-12-28','2016-12-27','2017-12-27','2018-12-27','2019-12-27','2020-12-26',
        '2021-12-26','2022-12-26','2023-12-26','2024-12-25','2025-12-25','2026-12-25','2027-12-25','2028-12-24','2029-12-24','2039-12-22','2049-12-19',
        '2059-12-17','2069-12-14','2079-12-12','2089-12-09','2099-12-07']

    fig=plt.figure(figsize=(20,12))
    plt.subplots_adjust(left=0.1,  bottom=0.1,  right=0.9, top=0.9, wspace=0.4, hspace=0.4)
    k=0
    for t in times:
        k+=1
        mat1=df1[['I', 'J', 'K', 'SGAS@'+t,'PORV']].to_numpy()
        mat2=df2[['I', 'J', 'K', 'SGAS@'+t,'PORV']].to_numpy()
        Sgas1=[]
        Sgas2=[]
        for i in range (20):
            temp1= mat1[mat1[:, 1] == i+1]
            temp1=np.c_[ temp1, np.zeros(np.shape(temp1)[0]) ]
            temp1[:,5]=temp1[:,3]*temp1[:,4]
            SUM=np.sum(temp1,axis=0)
            Sgas1.append(SUM[5])
            temp2= mat2[mat1[:, 1] == i+1]
            temp2=np.c_[ temp2, np.zeros(np.shape(temp2)[0]) ]
            temp2[:,5]=temp2[:,3]*temp2[:,4]
            SUM=np.sum(temp2,axis=0)
            Sgas2.append(SUM[5])
            plt.subplot(5,8,k)
        plt.plot(np.arange(1,21,1),Sgas1,color='b')
        plt.plot(np.arange(1,21,1),Sgas2,color='r')
        plt.ylim(0,1200000)
        plt.xlim(1,20)
        plt.title(str(t), fontsize=10)
    fig.suptitle(str(folder1)+str(folder2))
    plt.savefig('test_profiledouble.pdf', format = 'pdf' ,dpi=fig.dpi)

```

Figure 9: Plume Profile code

4 Results and Discussion

Results from reservoir simulations will be presented and discussed in this section. 16 different scenarios were made and run on both thermal and isothermal modes on the pflotran-OGS reservoir simulator.

4.1 Injection Temperature

The ambient temperature of the formation varies between 56 and 58 degrees Centigrade. Four different injection temperatures are studied. Although varying CO_2 temperature can have great effects on the gas phase viscosity and density, comparing the simulation results in different time steps does not show very specific variation in plume shape. Figure 13 illustrates the gas saturation at the end of the eighth year, in a cross-section including the well for all injection temperatures. In the case with the coldest injection, 15 degrees Centigrade, CO_2 saturation around the well is more than in other cases, this phenomenon is due to the lower $CO_2 - brine$ density difference, which decreases the gravitational forces and makes the upward movement less than other cases. This trend is valid for other temperatures too, meaning the higher the injection temperature, the lower the gas saturation in the vicinity of the well.
Results from the simulations in the long term do not show any significant differences between different cases. This could be due to different reasons. One important reason could be the very big surface-to-volume ratios of the porous media. Injected CO_2 reaches an equilibrium temperature very fast, and the temperature front does not move as far and fast as the gas front. Consequently regardless of the injection temperature, free gas will have approximately the same properties in all cases in the long term and far from the injection point.

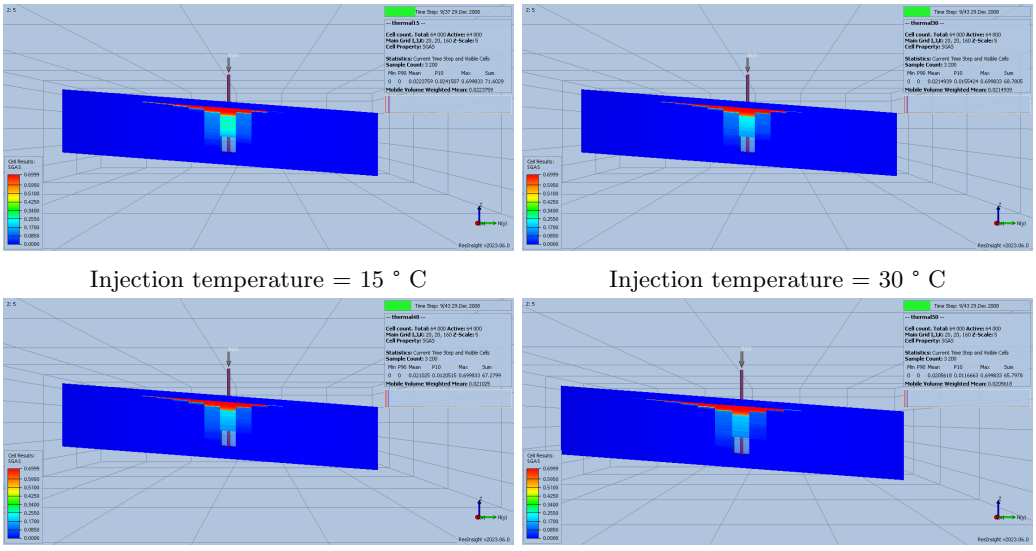

Injection temperature = 15 ° C | Injection temperature = 30 ° C

Injection temperature = 40 ° C | Injection temperature = 50 ° C

Figure 10: Gas saturation distribution at the end of the eighth year

4.2 Injection Pattern

Figure 11 shows the cumulative amount of gas injected into the reservoir. In one case, CO_2 is injected continuously for seven years, and in the second case, the well is shut and opened periodically. This figure proves that the modifications in the well schedule were done correctly, as the cumulative amount of gas injected is the same for both cases.
Comparing the results from thermal and isothermal simulations in the periodic case does not show any specific differences. In the short term, less than fourteen years when the total amount of injected gas in two cases is not equal yet, it is clear that the plume propagation in both the

horizontal and vertical directions will be different. So comparing these two cases in the short term is not logical.
Comparing the time, when these two cases reach the reservoir boundary, shows that the plume in the periodic system reaches the boundary one year later than the constant injection. Although increasing the time by which the plume reaches the boundary could be beneficial regarding the storage capacity, the higher operational expenses should be considered.

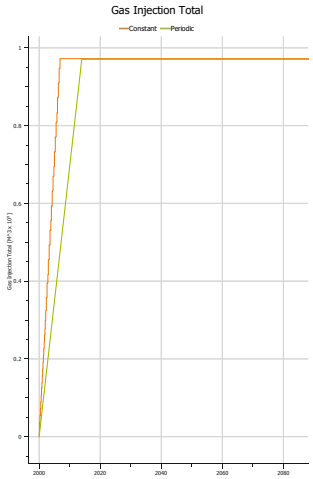

Figure 11: Cumulative injected gas

4.3 Brine Salinity

Brine density is known in most of the production sites, which is found from water samples, or petrophysical data, but for CO_2 sequestration projects, it is not determined. Results from simulations for three different brine salinities are studied carefully. As expected, changes in this property would affect the brine properties, like viscosity and density, and also alter the amount of gas that can be dissolved in the aqueous phase. Brine density, viscosity, and maximum mole fraction of gas dissolved in the brine are given in the table 4.

Case no.	Salinity[Molal]	Density[kg/m^3]	Viscosity[cP]	Dissolved gas[-]
1	1	1028	0.62	0.01993
2	1.2	1036	0.64	0.01909
3	1.4	1043	0.65	0.01828

Table 4: Brine properties for three brine salinity

Comparing the results regarding the plume shape, plume movement, and amount of dissolved gas in the brine, does not show any specific difference between these cases. Moreover, running simulations in isothermal or non-isothermal modes does not make any difference. Figure 12 shows the mole fraction of CO_2 in brine for a specific time step.

Although a very small alteration in the amount of dissolved gas is observed in various cases, which affects the amount of free gas, and brine properties, which can end up in changes in the viscous and buoyancy movement of the plume, there is no clear difference between cases. It can be concluded that changes in the brine salinity at least in this scale do not have a great influence on the final results.

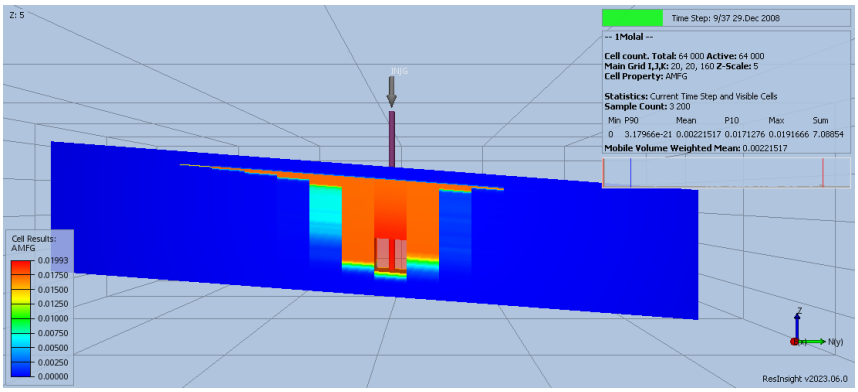

Brine Salinity = 1 Molal

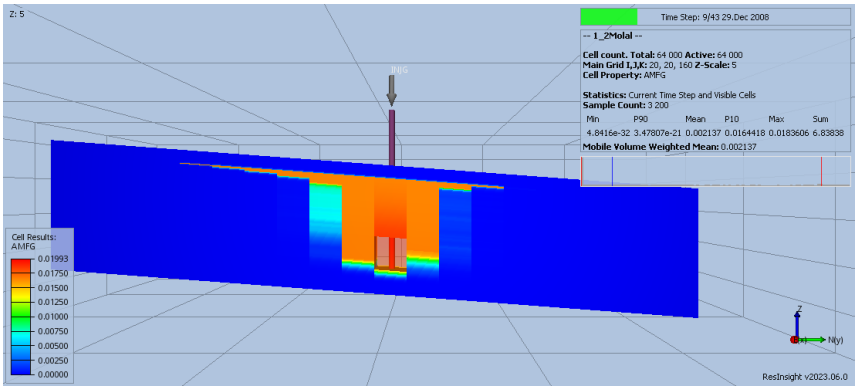

Brine Salinity = 1.2 Molal

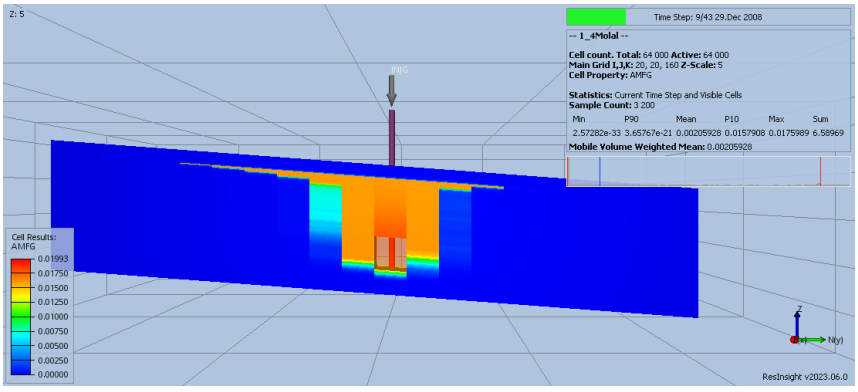

Brine Salinity = 1.4 Molal

Figure 12: Mole fraction of dissolved gas in aqueous phase

4.4 Permeability Anisotropy

Closely comparing the result of five scenarios with changes in vertical to horizontal permeability displays plume shape alteration in the short term. The higher the vertical permeability, the faster the plume ascends, so the plume is more propagated in the vertical direction in cases with lower vertical permeability. However, the plume shape in the long term is not a function of this property, because no matter how big this property is, the free gas will move to the shallowest part of the formation, and the plume shape will be highly dependent on other rock properties like the porosity of reservoir, and the irreducible water saturation. This phenomenon is observed in this study, too. But it should considered that easier movement of the free gas to the shallower parts decreases the time in which the free gas reaches the boundaries, which is an important subject in calculating the storage capacity. The results regarding the boundary reach will be discussed later.
Including the thermal effects in the simulations does not affect the plume shape either, which was expected.
One more thing that is neglected in this study is that changing the permeability ratio without changing the porosity of the reservoir would not be realistic. Moreover, permeability ratios could differ from layer to layer, so changing this property for the whole reservoir would cause a more significant change in the plume shape in the short term. Figure **??** shows the plume shape for four different scenarios in a constant time.

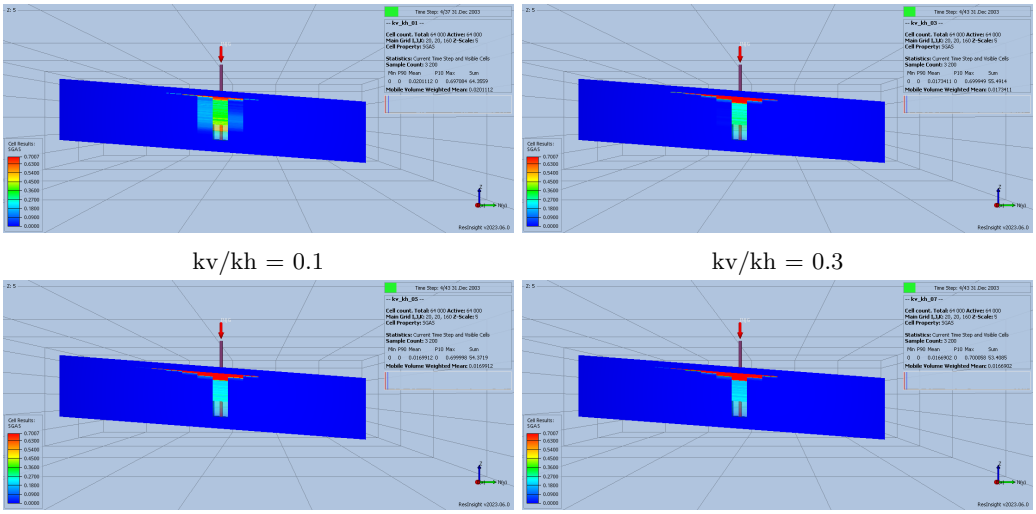

kv/kh = 0.1 kv/kh = 0.3

kv/kh = 0.5 kv/kh = 0.7

Figure 13: Gas saturation distribution at the end of the third year

4.5 Impermeable layers

In this part, in the first part, each case is compared based on being isothermal or thermal. in the second step, the effect of the chimney will be discussed.

In the first case, where there are fully impermeable layers, with no opening in any of them. This means that part of the CO_2 will be injected into this layer, with no pressure or mass communication with other layers. The amount of CO_2 injected is a function of the thief zone thickness. If the thief zone reaches the higher pressure limit, the well will stop injecting, which can affect the storage capacity. Comparing the isothermal and thermal results of the first scenario, there are small differences in CO_2 distribution in the well vicinity. In this case, running simulations in thermal mode does not considerably influence the plume propagation. Figure 14 displays the plume shape in a constant time step for two cases.

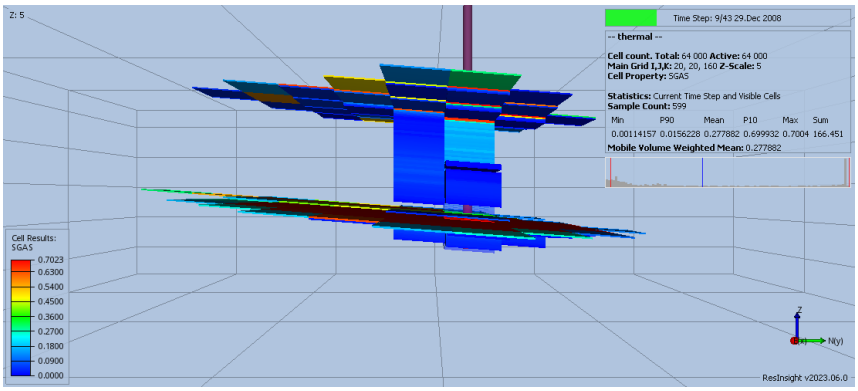

Thermal

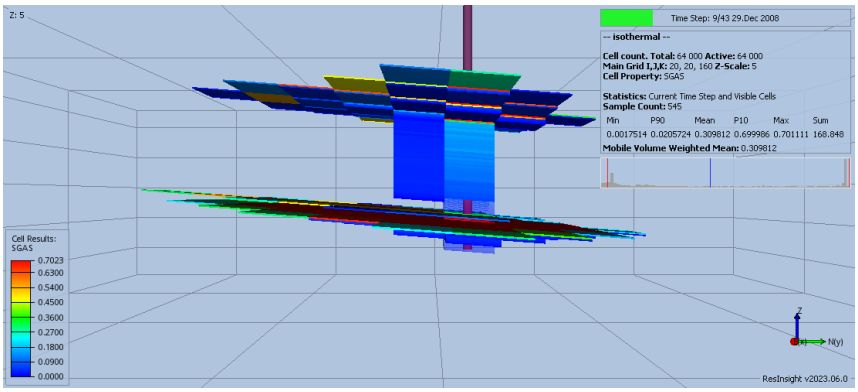

Isothermal

Figure 14: Gas saturation distribution at the end of the eighth year

In the second case, the thief zone is in pressure and mass communication with the shallower part of the reservoir, which will make the amount of the injected CO_2 in that layer more. However, the injected CO_2 will not reside in that zone and will move to the reservoir top. In this case, the plume shape is very different from previous cases, but the thermal and isothermal simulations do not have significant differences. This could be due to the distance between the chimney and the injection point because the free gas that reaches the chimney is in thermal equilibrium with the formation rock, which is far from the critical point of the carbon dioxide. Figure 15 shows the plume shape for the same case with two different modes, thermal and isothermal.

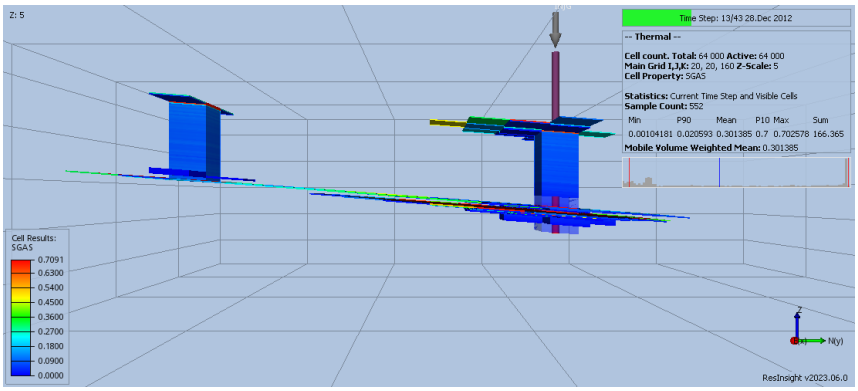

Thermal

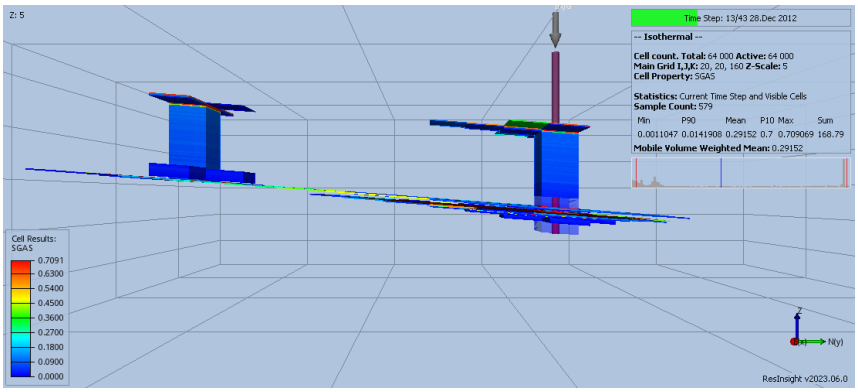

Isothermal

Figure 15: Gas saturation distribution at the end of the twelfth year

4.6 Plume Profile

Figure 16 shows the results from the code generated for the plume profile, which is used to compare two cases. Both colors are for the same case, but the blue line represents the thermal simulation and the red one is for isothermal.

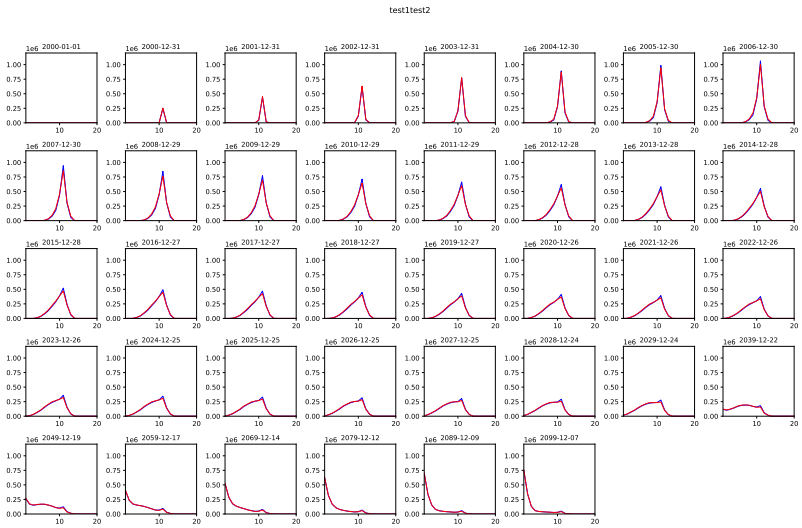

Figure 16: Plume profile for base case(thermal and isothermal)

5 Conclusion

Based on the results from reservoir simulations, it can be concluded that running the CO_2 sequestration simulations on thermal mode is not necessary for the case discussed in this work. However, this conclusion can not be expanded to all cases. Including thermal equations for cases in which the reservoir and injection pressure and temperature are close to the critical point of CO_2, where injected gas might have abrupt phase changes from liquid-like to gas-like, could be beneficial. Moreover, three moving fronts, pressure, free gas, and temperature do not move together, and this causes the injected CO_2 to move in a temperature close to the reservoir's initial temperature. Reducing the cell sizes along the horizontal axis could enhance the detection of thermal effects, as larger grid sizes may hinder the detailed examination of temperature variations. Running simulations on thermal mode for real-life cases, with a very high number of cells can considerably increase the computational costs, so it should be closely investigated. In considering future directions for research, it is essential to explore additional aspects that can enhance the robustness and applicability of the findings. The following outlines potential areas for further investigation and expansion of the current study, altering the reservoir's initial pressure and temperature closer to the critical point of CO_2, lowering the size of grid cells, adding more heterogeneity to the formation, including faults, and chimneys.

Bibliography

[1] URL: https://docs.opengosim.com (visited on 19th Dec. 2023).

[2] Niemi Auli, Bear J and Bensabat J. *Geological storage of CO2 in Deep Saline Formations.* 2017.

[3] M Dentz and D.M. Tartakovsky. 'Abrupt-interface solution for carbon dioxide injection into porous media'. In: *Transport in Porous Media* (2009).

[4] henhao Duan and Rui Sun. 'An improved model calculating co2 solubility in pure water and aqueous nacl solutions from 273 to 533 k and from 0 to 2000 bar'. In: *Chemical geology* (2003).

[5] Zhenhao Duan et al. 'densities of the co2–h2o and co2–h2o–nacl systems up to 647 k and 100 mpa'. In: *Energy & Fuels* (2008).

[6] Julio Enrique Garcia. 'Fluid Dynamics of Carbon Dioxide Disposal into Saline Aquifers'. In: (2003).

[7] Wu Haiqing, Bai Bing and Li Xiaochun. 'An advanced analytical solution for pressure build-up during CO2 injection into infinite saline aquifers: The role of compressibility'. In: *Advances in Water Resources* (2017).

[8] John Houghton. 'Global warming'. In: *Reports on progress in physics 68 1343* (2005).

[9] Samuel Krevor et al. 'Capillary trapping for geologic carbon dioxide storage – From pore scale physics to field scale implications'. In: *International Journal of Greenhouse Gas Control* (2015).

[10] B. Metz et al. 'IPCC special report on carbon dioxide capture and storage.' In: *Cambridge University Press* (2005).

[11] Bamshad Nazarian and Anne Kari Furre. 'Simulation Study of Sleipner Plume on Entire Utsira Using A Multi-Physics Modelling Approach'. In: *GHGT-16* (2022).

[12] J.M. Nordbotten and H.K. Dahle. 'Impact of the capillary fringe in vertically integrated models for CO2 storage'. In: *Water Resource Research* (2011).

[13] JAN MARTIN NORDBOTTEN and MICHAEL A. CELIA. 'Similarity solutions for fluid injection into confined aquifers'. In: *Journal of Fluid Mech* (2006).

[14] JAN MARTIN NORDBOTTEN, MICHAEL A. CELIA and STEFAN BACHU. 'Injection and Storage of CO2 in Deep Saline Aquifers: Analytical Solution for CO2 Plume Evolution During Injection'. In: *Transport in Porous Media* (2005).

[15] World Energy Outlook. In: (2023).

[16] S. Pacala and R. Socolow. 'Stabilization Wedges: Solving the Climate Problem for the Next 50 Years with Current Technologies'. In: *Science* (2004).

[17] Catriona Reynolds and Samuel Krevor. 'Characterizing flow behavior for gas injection: Relative permeability of CO2-brine and N2-water in heterogeneous rocks'. In: *Water Resource Research* (2015).

[18] Philip Ringrose. *How to Store CO2 Underground: insights from early-mover CCS Projects.* Springer, 2020.

[19] Semere Solomon. 'CO2 Storage: Case Study on the Sleipner Gas field in Norway'. In: *The Bellona Foundation* (2007).

[20] Roland Span and Wolfgang Wagner. 'A new equation of state for carbon dioxide covering the fluid region from the triple-point temperature to 1100 k at pressures up to 800 mpa'. In: *Journal of physical and chemical reference data* (1996).

[21] Bachu Stefan. 'Screening and ranking of sedimentary basins for sequestration of CO2 in geological media in response to climate change'. In: *Environmental Geology* (2003).

[22] V. Vilarrasa et al. 'Semianalytical Solution for CO2 Plume Shape and Pressure Evolution During CO2 Injection in Deep Saline Formations'. In: *Transport in Porous Media* (2013).